Towards Biophysically-Based Neuromorphic Computing at Scale: Markov Abstractions of Electrochemical Reaction-Diffusion in Synaptic Transmission

Margot Wagner [1,2,3], **Thomas M. Bartol** [3,4], **Terrence J. Sejnowski** [2,3,4,5], **and Gert Cauwenberghs** [1,2*]

[1] *Department of Bioengineering, University of California, San Diego, La Jolla, CA, USA*
[2] *Institute for Neural Computation, University of California, San Diego, La Jolla, CA, USA*
[3] *Computational Neurobiology Laboratory, Howard Hughes Medical Institute, The Salk Instutute for Biological Studies, La Jolla, CA, USA*
[4] *Center for Theoretical Biological Physics, University of California, San Diego, La Jolla, CA, USA*
[5] *Division of Biological Sciences, University of California, San Diego, La Jolla, CA, USA*

Correspondence*:
Gert Cauwenberghs, Integrated Systems Neuroengineering Lab, University of Calfirnia, San Diego, Department of Bioengineering, 9500 Gilman Dr, La Jolla, CA 92093
gert@ucsd.edu

ABSTRACT

Progress in computational neuroscience towards understanding brain function is challenged both by the complexity of molecular-scale electrochemical interactions at the level of individual neurons and synapses, and the dimensionality of network dynamics across the brain covering a vast range of spatial and temporal scales. Our work abstracts the highly detailed, biophysically realistic 3D reaction-diffusion model of a chemical synapse to a compact internal state space representation that maps onto parallel neuromorphic hardware for efficient emulation on very large scale, and offers near-equivalence in input-output dynamics while preserving biologically interpretable tunable parameters.

Keywords: neuromorphic, synapse, Markov chain, Monte Carlo

1 INTRODUCTION

Neuromorphic engineering pursues biological inspiration for computational intelligence by emulating neural circuits in silicon very large-scale integrated (VLSI) circuits (Mead (1990)). Practical instantiations of neuromorphic silicon circuits have varied in their biological realism, with more realistic Hodgkin-Huxley type models being difficult to implement and not as scalable, while less realistic integrate-and-fire (I&F)

architectures being easier to implement but not readily adjustable with parameters that are non-mechanistic and do not the capture complex dynamics of neural networks (Poon and Zhou (2011), Indiveri et al. (2011)). Even Hodgkin-Huxley models lack the detail at the subcellular scale that we understand exists today.

Synapses form the connections between neurons and the strength of these connections changes over time, forming the basis of learning and memory in both biological and artificial neural networks. The computations in synapses are highly nonlinear in nature, but in artificial neural networks, synaptic strength is typically reduced to a single value, which is updated to a specific task. The learning rule for synaptic strength is typically updated globally or more recently with spike-time dependent plasticity rule, which have a strong biological backing (Pedroni et al. (2019)). Limitations in synaptic representation and computation in VLSI restrict the potential computing power of neuromorphic systems and restrain achievable benchmarks compared to the low power and parallelism of an actual brain. Our work addresses the need for a more biophysically realistic model of the synapse with biologically tunable parameters to represent synaptic plasticity, while offering efficient real-time implementation in neuromorphic architecture.

Synaptic transmission is dictated by a series of events initiated by presynaptic stimulation in the form of action potentials. An action potential causes membrane depolarization which leads to stochastic opening and closing of voltage-dependent calcium channels (VDCCs) lying on the presynaptic membrane and a resulting influx of calcium to the presynaptic terminal. Neurotransmitter release is modulated by calcium binding to calcium sensors near the neurotransmitter filled vesicles at the active zone, but calcium has other fates as it diffuses from the VDCCs. In addition to binding to the calcium sensors, it can bind to calbindin, which acts as a buffer, or it can be removed by plasma membrane calcium (PMCA) pumps. If enough calcium is able to bind to the calcium sensors, though, then neurotransmitters are released across the synaptic cleft and initiate downstream effects at the postsynaptic membrane. This process of synaptic transmission is the basis of learning and communication in the brain.

Abstracting this for computational efficiency, we created a series of Markov state transitions to fully realize the system with multiple internal states done in Python allowing for a biophysically tunable model of synaptic connectivity implementable in neuromorphic architectures.

2 MATERIALS AND METHODS

2.1 Markov Chain Models

The cascade of events from the action potential stimulus input to the presynaptic neurotransmitter release output can be equivalently modelled as Markov chain to fully realize the system with multiple internal states instead of directly tracking all molecules and their kinetics in a computationally complex spatiotemporal 3D reaction-diffusion model. Each internal Markov state is assumed to be dependent solely on the state at the previous timepoint and is conditionally independent of all previous timepoints, simplifying simulations. Therefore, the fully biophysically complex system of synaptic transmission can be abstracted and sampled to create a Markov Chain Monte Carlo (MCMC) which answers the same question of neurotransmitter release utilizing tunable biophysical parameters while allowed scalability for implementation in neuromorphic architectures.The MCMC was implemented in Python using state transition models creating more efficient simulation for internal states of the presynaptic terminal and nuerotransmitter release due to stimulus input.

For any given stimulus input, the VDCCs are assigned transition probabilities between states based on a five-state kinetic model (Figure 1, replicated from Bartol et al. (2015) with permission) found experimentally and validated computationally with four closed states and a single open state (Bischofberger et al. (2002), Church and Stanley (1996), Bartol et al. (2015)). Prior to the stimulus, all VDCCs begin in a

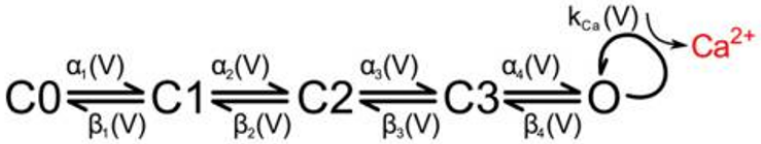

Figure 1. State diagram for voltage-dependent calcium channels and resulting calcium influx in the presynaptic membrane, Bartol et al. (2015).

closed state, and the concentration of calcium in the presynaptic terminal is at steady-state. The transition probabilities are voltage dependent akin to a Hodgkin-Huxley model where the number of open VDCCs at any given moment is used to determine the number of calcium entering the presynaptic terminal based on experimental I-V curves and the resulting I-V equation found in Bischofberger et al. (2002). Calcium influx is captured similarly by including transitions from the open VDCC state to the open VDCC state and an internal calcium generation. Using this, influx of calcium is modelled over the entire stimulus input due to VDCC opening.

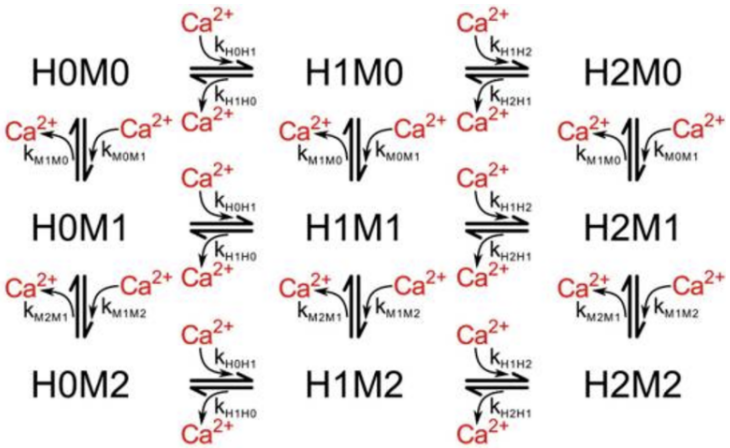

Figure 2. State diagram for calbindin binding, Bartol et al. (2015).

Once calcium has entered the presynaptic terminal, much of it binds to calbindin, which acts as a buffer and primarily modulates the amount of calcium that is able to reach the calcium sensors at the active zone. The state transitions are reversible first-order reactions, thus transition probabilities are dependent of the free calcium in the system and are updated as that amount changes over time. Calbindin has four binding sites, two high affinity sites and two medium affinity sites, leading to a nine-state calcium concentration-dependent kinetic model (Figure 2, , replicated from Bartol et al. (2015) with permission) (Nagerl et al. (2000)). By modelling the binding and unbinding of calcium to calbindin as a loss or gain of free calcium respectively, calcium transients can also be elucidated.

Our Markov chain is a discrete-state chain in discrete time. Markov chains are modelled by a probability that the chain will move to another state given its current state and is conditionally independent of all previous timesteps. The probabilities are by nature only dependent on the current state of the Markov chain, thus:

$$P(X_{n+1} = j|X_n = i, X_{n-1}, ..., X_o = i) = P(X_{n+1} = j|X_n = i) = P_{ij} \tag{1}$$

For state transitions, the probability is the transition rate times the time step. In the case of calbindin transitions, this is further multiplied by the amount of free unbound calcium for forward reactions. In the case of a multistate system, this gives a transition probability matrix for the likelihood of transition from a given state at the current timestep to any other state at the next timestep. This matrix is sparse, with nonzero probabilities only for adjacent states where transition is possible. In the case of the five-state VDCC system, this gives

$$P_{ij} = \begin{cases} k_{ij}\Delta t & i \neq j, i = j \pm 1 \\ 0 & i \neq j, i \neq j \pm 1 \\ 1 - \sum_{j=0}^{N} P_{ij} & i = j \end{cases}$$

Typically Markov state transitions are modelled via discrete inverse transform method, where given a random variable X to describe the transitions with probability $P(X = x_i)$, and $P(X = x_i)$ describes a partition of unity (Figure 3). Therefore, we can generate a random number uniformly, $R \sim U(0, 1)$ and map it into discrete values of X. For example, in a two state system, $X_j = 0$ if $R \leq P_{i,0}$ or $X_j = 1$ if $P_{i,0} < R \leq P_{i,0} + P_{i,1} = 1$. This involved searching the state space for the next state given the current state for each molecule in the system at each timestep, which can be a slow process for systems with a large number of states and molecules.

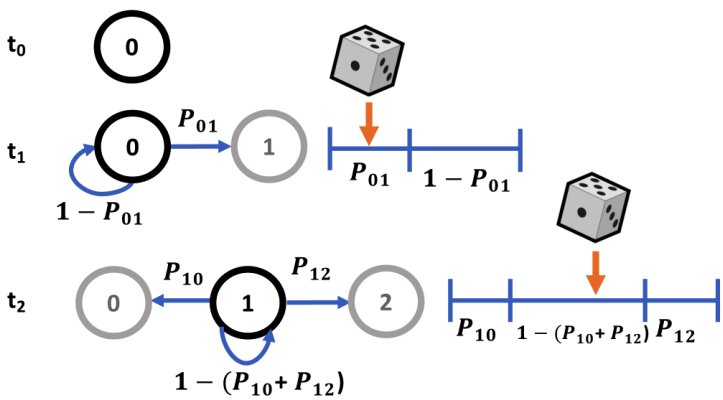

Figure 3. Markov sampling scheme for state transitions.

Here we have implemented an optimized MCMC sampling strategy involving sampling from a multinomial distribution, where $X \sim Multi(n, \mathbf{p})$ with the probability mass function for n experiments each with one of p possible outcomes:

$$f(x_1, ..., x_k; n, p_1, ...p_k) = \frac{n!}{x_1!...x_k!} p_1^{x_1} \times ... \times p_k^{x_k} \tag{2}$$

At each time point, the number of transitioning molecules of interest is n while the transition probabilities, whether voltage or concentration dependent, are $\mathbf{p}$. This expedites computation by only requiring a single computation at each time.

2.2 MCell Models

MCell is a modelling software that uses spatially realistic 3D geometries and Monte Carlo reaction-diffusion modelling algorithms, which allows for biophysically realistic simulations of high complexity as it specifically tracks the state of every molecules in space and time (Bartol et al. (2015)). Due to the accuracy and specificity, it provides a ground truth for biological simulations but does so at the cost of computational complexity.

To validate and compare our Markov models of synaptic transmission, we built a biophysically realistic stochastic 3D reaction-diffusion system with all major components for presynaptic vesicle release variability in response to a stimulus input (Figure 4). The model included realistic geometry for a CA3-CA1 *en passant* synapse with parameters set from experimental data (Nadkarni et al. (2010), Bartol et al. (2015)). The CA3-CA1 synapse was chosen for the simulations as it is highly studied experimentally and is important for learning and memory. All kinetics and parameters match those used for the equivalent Markov models.

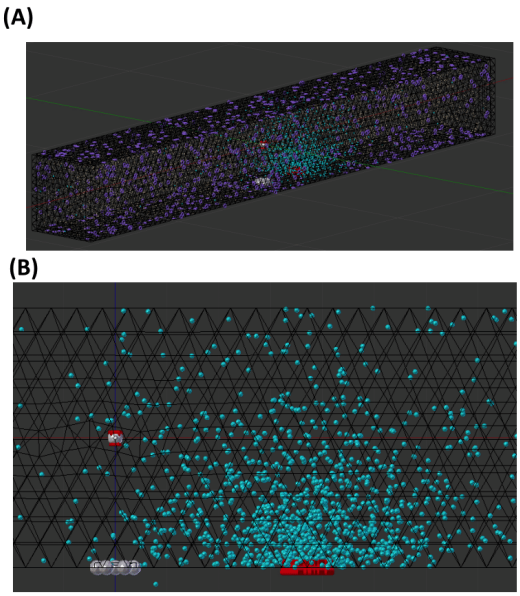

Figure 4. MCell model for synaptic transmission containing voltage-dependent calcium channels (red), calcium (blue), calcium sensors (grey), and plasma membrane calcium pumps (purple). Calbindin not pictured here due to their large number.

The MCell model includes the canonical presynaptic geometry for an average terminal as a rectangular box measuring 0.5μm by 0.5μm by 4μm containing the calbindin buffer, steady-state calcium concentration, PMCA pumps, VDCCs and calcium sensors modulating neurotransmitter release (Nadkarni et al. (2010)). The detailed kinetics of these systems have been discussed in detail elsewhere and are based on experimental data (Bartol et al. (2015)). The active zone is based on that of an average presynaptic active zone with only one being including and containing seven docked neurotransmitter vesicle release sites. The VDCCs of type P/Q and are stationed at a biophysically realistic distance from the active zone, also located on the membrane. PMCAs are homogenously placed across the presynaptic membrane while calbindin are placed in the volume. This is a flexible architecture that can respond to any stimulus input and allows for

monitoring of that states of each molecule in the system. To compare with the Markov models, we used the same single action potential stimulus.

3 RESULTS

3.1 Voltage-Dependent Calcium Channels

The efficient Markov chain implementation has strong agreement with the full MCell model in terms of the internal state transients in response to an external stimulus. Figure 5 shows the fraction of open VDCCs over time in response to the action potential, which controls the amount of calcium influx to the system. Transients for all states can be found in the supplemental material. As expected, the number of closed VDCCs (state C0) decreases over the duration of the stimulus. The internal states (C1-C3) subsequently increase and decrease as the membrane voltage increases and the forward rates for the VDCCs increase, leading to an exponential increase in the open VDCCs while the membrane depolarizes. At the maximum membrane potential, almost all VDCCs are in the open state. As the membrane repolarizes, the reverse reaction rates constants increase, and the VDCCs close. This leads to another increase and decrease in the internal VDCC states as the receptors go from their open to resting state (C0). While both the stochastic MCell and Markov simulations show strong agreement, the deterministic solution overestimates the amount of open VDCCs suggesting the importance of introducing stochasticity in the VDCC transitions.

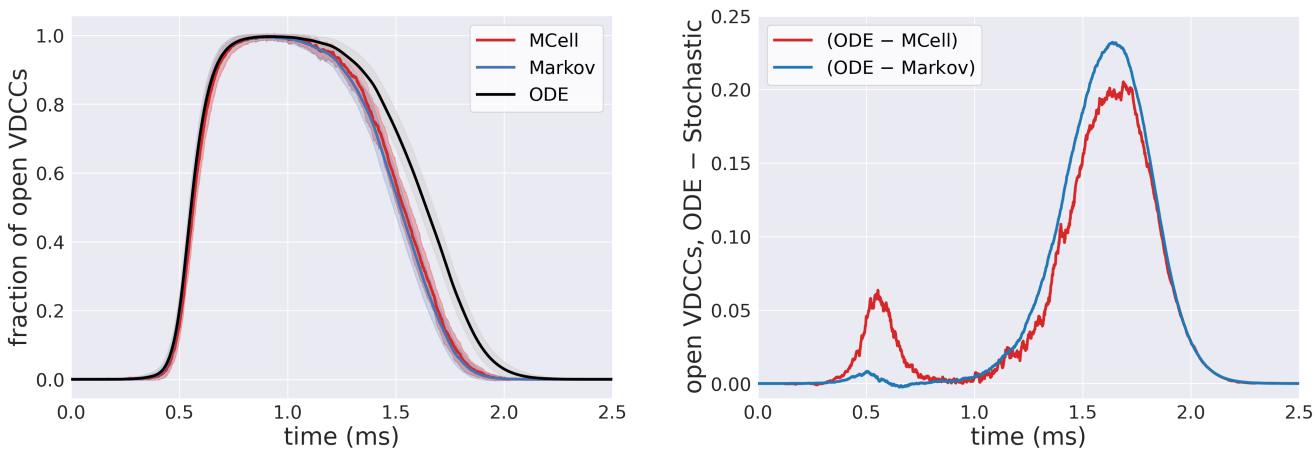

Figure 5. Fraction of open voltage-dependent calcium channels in response to action potential stimulus for stochastic MCell and Markov simulations and a deterministic ODE forward Euler simulation (*left*), and the difference between deterministic and stochastic simulations for fraction of open VDCCs for MCell and Markov (*right*).

In its open state, VDCCs allow for the probabilistic influx of calcium through the channels into the presynaptic bouton. This is exemplified in Figure 6, where there is an increase in the calcium influx through the open VDCCs over the course of the stimulus. Due to the overestimation of open VDCCs by the deterministic solution, there is a predicted to be larger number of calcium that enter the presynaptic terminal than for the stochastic simulations. This can have serious consequences as calcium directly modulates the neurotransmitter release on the presynaptic side. Therefore, an overestimation would predict a strong signal than would actually occur. Again, there is strong agreement between the more computationally complex MCell model and the computational efficient Markov equivalent model.

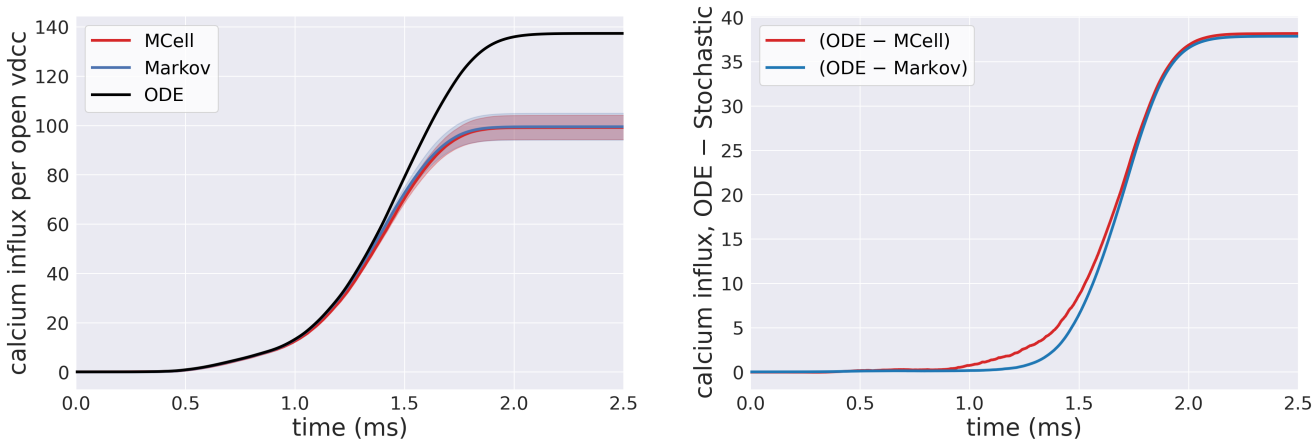

Figure 6. Calcium influx through open VDCCs in response to action potential stimulus for stochastic MCell and Markov simulations and a deterministic ODE forward Euler simulation (*left*), and the difference between deterministic and stochastic simulations for calcium influx for MCell and Markov (*right*).

3.2 Calbindin Buffer

Simulations of homogeneous calcium and calbindin were run using both the MCell, Markov and deterministic simulation schemes. In the presence of calcium, the forward binding reaction is heavily favored and this is highlighted in Figure 7 where free calcium exponentially decreases. A similar transient is apparent for the unbound state of calbindin, as it quickly transitions to different stages of high and medium binding. While over the course of the simulation, all the free calcium is removed from the system, calbindin states reach a new steady-state where there are still unbound calbindin. Similarly, the fully bound state, H2M2, rapidly increases and reaches a new steady state that is still only 1% of all calbindin. This is due to the high concentration of calbindin in the presynaptic bouton. Even once all the calcium is in a bound state, there is plenty of unbound or partially bound calbindin remaining in the system. Calbindin acts as a strong buffer allowing for calcium storage and asynchronous neurotransmitter release, so this and slow unbinding rates becomes an important feature of calbindin. The rapid extent to which calcium binds to calbindin shows the impact of buffering on calcium's ability to diffuse and bind to the calcium sensors in the active zone. The inclusion of calbindin at such high concentrations becomes a key feature of maintaining the relatively low release rates of neurotransmitters even in the presence of a stimulus.

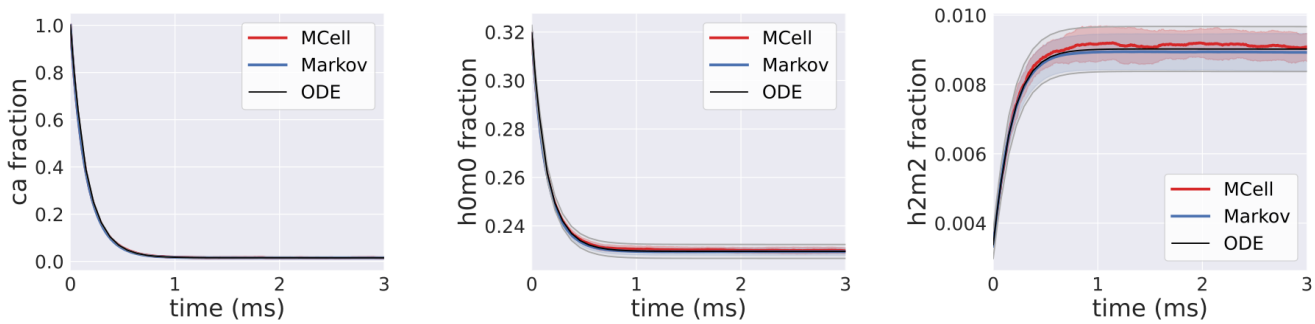

Figure 7. Transients for homogeneous calcium-calbindin buffer binding in the presynaptic bouton for free calcium *(left)*, the unbound calbindin state, H0M0 *(middle)*, and the fully bound calbindin state, H2M2 *(right)*

3.3 Benchmarks

Runtime and total floating point operations were used as metrics for comparison between the simulation methods (Figure 8). Here we compare MCell, the standard Markov model, and the multinomial Markov stochastic models. The deterministic Euler solution is included as well for a standard comparison, although it has been shown there is some accuracy loss for the deterministic solutions. For the VDCC simulations, the optimized multinomial sampling Monte Carlo Markov chain model has a runtime on the order for the forward Euler deterministic solution. The MCell and standard Markov stochastic models exemplify a runtime an order of magnitude higher. The number of operations is also much high for the standard Markov model as compared to the multinomial Markov model. Operations were not included for MCell as there is currently no method to measure FLOPs for the software.

VDCC	Runtime	Floating Point Operations
MCell	139.20 ± 7.0 s	--
Standard Markov	109.16 ± 0.93 s	7.01 (± .02)E+07
Multinomial Markov	9.40 ± 0.08 s	1.26(± .01)E+07
*ODE (Euler)**	*10.05 ± 0.13 s*	*7.73E+06*

Calbindin	Runtime	Floating Point Operations
MCell	29.34 ± 0.39s	--
Standard Markov	4.10E+4 s	4.612 (± .002) E+07
Multinomial Markov	2.37 ± .02 s	2.72E+07 (± 8E+03)
*ODE (Euler)**	*0.72 ± 0.01 s*	*1.60E+06*

* accuracy loss with deterministic solution

Figure 8. Benchmarks for different simulation types for both voltage-dependent calcium channel and calbindin binding simulations.

For the calbindin model, the multinomial Markov method is again an order of magnitude faster than the MCell model although it is also an order of magnitude slower than the deterministic model. The standard Markov model is four orders of magnitude slower than the multinomial model due to the high density of calbindin molecules in the simulation. This highlights the importance of our multinomial sampling scheme for simulations with large numbers of molecules and multiple states. The operations are also fewer for the multinomial case than the standard case. Overall, the multinomial Markov simulation provides a computationally efficient alternative to stochastic MCell simulations while maintaining the biological accuracy.

4 DISCUSSION

The goal of this work was to create a more computational efficient model of biologically realistic synaptic transmission for use in large scale neuromorphic systems. We created a multinomial Markov Chain Monte Carlo (MCMC) sampling strategy for capturing the internal states of vital molecules in the system in response to stimulus where transition probabilities could be voltage- or concentration-dependent and the next timestep could be predicted solely using the current timestep. This scheme was implemented

to capture the dynamics of the stochastic opening and closing of voltage-dependent calcium channels (VDCCs) through multiple internal states as well as the resulting calcium influx into the presynaptic bouton through the open VDCCs. Once calcium has entered the presynaptic terminal, we also simulated calcium binding to the calbindin buffer which modulates calcium levels in the bouton, directly impacting the amount of calcium that reaches the calcium sensors in the active zone. This amount impacts the neurotransmitter release from the presynaptic side and the resulting effects on the postsynaptic side.

All simulations were modelled using the optimized multinomial Markov sampling method as well as a typical Markov sampling method and compared to highly detailed 3D geometric stochastic reaction-diffusion simulations done using MCell. The Markov simulations show agreement with the MCell simulations for the system dynamics including the number of open VDCCs and calcium influx in response to an action potential stimulus as well as the binding of calcium to the calbindin buffer. Differences are observed from the deterministic solution to the stochastic simulations implying the importance of stochasticity in these simulations to capture more biologically-realistic systems.

Exemplified by runtime and total number of operations, the optimized multinomial MCMC method of simulations was shown to be more efficient than the standard Markov model while being faster than the MCell equivalents. This is hopeful for scaling these biologically-realistic models to large-scale systems while maintaining biological tunability.

Next steps involve capturing modelling the remaining kinetics in a similar fashion including the binding and removal of calcium by the plasma membrane calcium (PMCA) pumps as well as binding to the calcium sensors. In addition, to capture the diffusion of calcium through the presynaptic terminal but specifically to the calcium sensors at the active zone, a diffusive kernel must be included to the system. Upon inclusion of these elements, the entire process from stimulus to neurotransmitter release can be modelled as a series of Markov chains leading to powerful implications for synaptic transmission modelling. The entire synapse can be included as well with the inclusion of a diffusive kernel across the synaptic cleft as well as downstream effects on the postsynaptic side, of which many mirror similar kinetics and dynamics as the presynaptic side leading to a natural extension of this modelling framework. The resulting system would be a biologically tunable model of synaptic transmission for any stimulus input in a highly efficient manner. This opens the door for large-scale implementations of synaptic transmission and learning readily implementable into neuromorphic architectures with biological realism never before seen.

CONFLICT OF INTEREST STATEMENT

The authors declare that the research was conducted in the absence of any commercial or financial relationships that could be construed as a potential conflict of interest.

FUNDING

This work was supported by NSF Graduate Research Fellowship funding, the National Science Foundation and the Office of Naval Research.

REFERENCES

Bartol, T. M., Keller, D. X., Kinney, J. P., Bajaj, C. L., Harris, K. M., Sejnowski, T. J., et al. (2015). Computational reconstitution of spine calcium transients from individual proteins. *Frontiers in Synaptic Neuroscience* 7. doi:10.3389/fnsyn.2015.00017

Bischofberger, J., Geiger, J. R. P., and Jonas, P. (2002). Timing and efficacy of ca2+ channel activation in hippocampal mossy fiber boutons. *The Journal of Neuroscience* 22. doi:10.1523/JNEUROSCI.22-24-10593.2002

Church, P. and Stanley, E. (1996). Single l-type calcium channel conductance with physiological levels of calcium in chick ciliary ganglion neurons. *The Journal of Physiology* 496. doi:10.1113/jphysiol.1996.sp021665

Indiveri, G., Linares-Barranco, B., Hamilton, T. J., van Schaik, A., Delbruck, R. E.-C. T., Liu, S.-C., et al. (2011). Neuromorphic silicon neuron circuits. *Frontiers in Neuroscience* 5. doi:10.3389/fnins.2011.00073

Mead, C. (1990). Neuromorphic electronic systems. In *Proceedings of the IEEE*. vol. 78, 1629–1636

Nadkarni, S., Bartol, T. M., Stevens, C. F., Sejnowski, T. J., and Levine, H. (2010). Modelling vesicular release at hippocampal synapses. *PLoS Computational Biology* 6. doi:10.1371/journal.pcbi.1000983

Nagerl, U. B., Novo, D., Mody, I., and Vergara, J. L. (2000). Binding kinetics of calbindin-d28k determined by flash photolysis of caged ca2+. *Biophysical Journal* 79, 3009–3018. doi:10.1016/S0006-3495(00)76537-4

Pedroni, B. U., Joshi, S., Deiss, S. R., Sheik, S., Detorakis, G., Paul, S., et al. (2019). Memory-efficient synaptic connectivity for spike-timing- dependent plasticity. *Frontiers in Neuroscience* 13. doi:10.3389/fnins.2019.00357

Poon, C.-S. and Zhou, K. (2011). Neuromorphic silicon neurons and large-scale neural networks: challenges and opportunities. *Frontiers in Neuroscience* 5. doi:10.3389/fnins.2011.00108